Failure mechanisms and fatigue strength reduction factor of a Cr-Ni-Mo-V steel welded joint up to ultra-long life regime

Ming-Liang Zhu*, *Fu-Zhen* Xuan

Key Laboratory of Pressure Systems and Safety, Ministry of Education; School of Mechanical and Power Engineering, East China University of Science and Technology, Shanghai 200237, China

Abstract. It is known that welded joint is much "weaker" than base metal due to discontinuities of geometry, materials and residual stresses. It seems current international design rules do not adopt a uniform approach to weld efficiency, which is often defined as the ratio of the strength of a welded joint to the strength of base metal, in their guidance for creep and fatigue design of welds. This appears to be a great barrier for the application of nuclear welded structures which has a prolonged design lifetime of 60 years. In this work, fatigue strength reduction factor of a Cr-Ni-Mo-V steel welded joint, machined from welded steam turbine rotors for nuclear power plant, was investigated by performing axially push-pull cyclic loads tests with both cross-weld and pure base metal specimens up to very high cycle fatigue regime under ultrasonic frequency at ambient temperature. The effects of residual stress, strain localization, and micro-defects in mismatched steels on failure mechanisms of welds were discussed thoroughly. Results show that fatigue strength reduction factor is varied in the range of 0.95-0.975, and is found to be dependent on fatigue lifetime for the first time. It is indicated that variation of fatigue strength reduction factor are associated with transition of crack initiation from specimen surface in high cycle fatigue regime to interior micro-defects in very high cycle fatigue regime. Comparing existing codes and standards for fatigue design of welds with experimental data indicates the over-conservativeness of present code-based design method. This implies a micro-defect based fatigue design approach is required for long life safe and reliability of weldments.

1 Introduction

The weld efficiency or joint efficiency is often defined as the ratio of the strength of a welded joint to the strength of base metal, and is thus inclusive of tensile, fatigue and creep strength. The weld efficiency can be related to strength reduction factor of welded joint, as welded joint is much "weaker" than base metal due to discontinuities of geometry, materials and residual stresses. It seems that current international design rules do not adopt a uniform approach to weld efficiency in their guidance for creep and fatigue design of welds. Creep design of engineering structures at elevated temperatures based on ASME Section III [1] defines creep strength reduction factor (CSRF) based on weld metal only, while the fast reactor design code RCC-MR [2] defines weld efficiency based on welded joint. In case of the fatigue strength reduction factor (FSRF), the RCC-MR code recommends that the fatigue curve of weld joint has a scaling factor of 1.25 lower than the fatigue curve of base metal, indicating a weld efficiency of 80%, whereas the ASME Subsection NH suggests a constant FSRF factor of 2.0 on the fatigue strength of welded joint (weld efficiency of 50%). A precise and unified evaluation of weld efficiency with sound mechanistic representation and associated proper recognition of its role in joint design are of great significance in balancing design safety and conservatism of modern engineering components and structures under extreme service conditions.

It is highly recommended by many code and standards that the creep strength reduction factor needs to be determined by experiments. Otherwise, in case of difficulty in creep experiments or availability of materials, single empirical values are often employed in design analysis, i.e., the value of 0.8 (80%) is proposed by EN13445-3, DIN EN13480-3, and ASME Section III. Define CSRF as a simple value and treatment of strength reduction factor as constant have long been challenged in creep damage assessment of welds. Tu and Sandström [3, 4] evaluated the influence of stress multiaxility and the corresponding stress redistribution process of welded components on the determination of CSRF by both experimental and numerical simulations. The CSRF was later found to be a function of testing temperature and time, especially in some heat resistance steels where the time dependent damage of microstructures are indicative of CSRF variation [5]. Tabuchi and Takahashi [6] reported the reduction factor of 100,000 hours creep rupture strength of welded joint to base metal was 0.75 at 600°C and 0.7 at 650°C for a Modified 9Cr-1Mo Steel. A similar presentation of CSRF as a function of

* Corresponding author: mlzhu@ecust.edu.cn

temperature was also reported by them in welded joints of Grade 122 steel [7].

The design against fatigue of welds is currently enabled by various codes and recommendations with well-developed design and assessment approaches, such as safe life design and damage tolerant design [8]. The geometrical and structural factors of welded joint has developed into a notch-based fatigue design approach [9], also termed local stress or strain approach [10, 11], which, generally leads to costly over-design, has witnessed great effectiveness in both low cycle fatigue (LCF) and high cycle fatigue (HCF) regimes. It is generally accepted that there exists a transition of crack initiation modes from specimen surface in LCF and HCF regimes to interior micro-defects in very high cycle fatigue (VHCF) regime which is characteristic of ultra-long fatigue life (fatigue life higher than 10^7 cycles) under lower stress levels often below the traditional fatigue limit [12]. The change of the shape of S-N curves has attracted great interests in fatigue design [13, 14]. Sonsino [15] gave material and manufacturing dependent recommendations for design of components submitted to loadings below the knee point of the conventional S-N curve. Murakami [16] thought of material defects as the basis of fatigue design. The weld efficiency in LCF and HCF regimes is thus inferred different from the one in VHCF regime, a point that is lack of research and verification. Moreover, the distribution and maximum permissible size of weld imperfections, unfortunately, are not explicitly taken into account in current fatigue design standards.

Therefore, in the present work, axially loaded cyclic tests using both welded joint and base metal specimens of Cr-Ni-Mo-V steel welds were carried out up to the VHCF regime to evaluate the weld efficiency and its underlying mechanisms. The fatigue design of welds up to the VHCF regime was then discussed by comparing various existing codes and standards. Finally, potential improvements by incorporating the micro-defects into the code are discussed based on the present results.

2 Materials and experiments

2.1 Materials and specimens

The material investigated was a welded joint with the 25Cr2Ni2MoV steel being the base metal (BM). The weldment was prepared by the submerged arc welding (SAW) technique using a weld metal (WM) rich of Ni [17]. The forged BM was quenched and tempered with microstructures dominated by lathy tempered martensites. After the SAW process and a post weld heat treatment (PWHT) at 580°C for 10 hours (furnace cooling), the yield strength (YS) and ultimate tensile strength (UTS) of the welded joint at room temperature was 726 MPa and 778 MPa, respectively. The microstructures of the WM mainly contain tempered bainites with long and lathy shape. The heat-affected zone (HAZ) shows a combined tempered martensite and bainites. A detailed observation of microstructures, and the tensile and strain hardening behavior have been reported in our previous paper [17].

Cross-weld specimens for VHCF testing were machined from the welded joint, and BM samples were also prepared for comparison purposes. Fig. 1 shows the shape and dimensions of the specimens for fatigue testing. For the cross-weld samples, it is noted that the WM, HAZ, and some parts of the BM constitute the parallel section to ensure the same stress during cyclic test. The same dimensions were employed for pure BM specimens, as indicated in Fig. 1b.

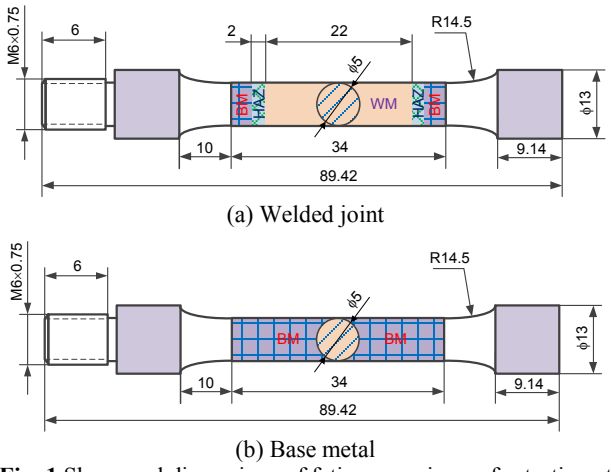

Fig. 1 Shape and dimensions of fatigue specimens for testing at 20 kHz: (a) cross-weld specimen, (b) pure base metal (dimensions in mm)

2.2 Fatigue testing methods

Prior to testing, all the specimens were mechanically polished. The final surface roughness of the specimen, R_a, is lower than 0.2 μm. Fatigue tests were then conducted on an ultrasonic system (USF-2000, Shimadzu, Japan) at ambient temperature with a frequency around 20 kHz. A pre-calibration process for the ultrasonic machine is required to establish a linear relationship between the horn side amplitude (in μm) and amplified output amplitude (in %), on which the determination of cyclic stress level is based. The load ratio of the test is -1. Compressive air was used to cool the middle part of the specimen to prevent the specimen from over-heating. In addition, an intermittent loading condition, i.e., 500 ms of pulse followed by 1000 ms of pause, was employed to minimize the thermal effect. As reported in [18], the thermal effect could be noticably reduced by employing cooling measures in a lower strength steel. After testing, all fracture surfaces of failed specimens were observed by scanning electron microscopy (SEM) in order to identify the crack initiation modes.

3 Results

3.1 *S-N* curve

Fig. 2 shows the *S-N* curves of the fatigue tests. It is noted that the *S-N* curves for both the two kinds of tests show a continuously decreasing mode. The traditional fatigue limit is not apparently observed. With the increasing of fatigue life, there exists a transition of crack initiation from specimen surface to interior micro-defects for cross-weld samples. While for the pure BM specimens, surface related fatigue cracking seems to be dominant as failure can occur at surface defect even at N_f of 10^8 cycles. Data from cross-weld samples have a more severe scatter than those of pure BM specimens. This is because, each part of the cross-weld samples has the potential to fatigue cracking, while the BM specimens can only fail at the BM. Apart from the *S-N* curve, another important difference between the two types of testing is the fatigue strength. It is obvious that the pure BM material has larger fatigue strength than that of cross-weld samples. This indicates the influence of welding process, i.e., welded joints always contain micro-defects, residual stress, and in particular, the mismatched structures. The strained welded joint will have more severe strain localization at weaker zone. A detailed discussion on the weld efficiency will be presented later. For comparison of fatigue strength, the results for pure BM and cross-weld specimens are then fitted as equations (1) and (2), respectively, as shown below.

$$\lg(\sigma_a) = 2.92367 - 0.04723\lg(N_f) + 0.00275\lg(N_f)^2 \quad (1)$$

$$\sigma_a = 602.3(N_f)^{-0.0089} \quad (2)$$

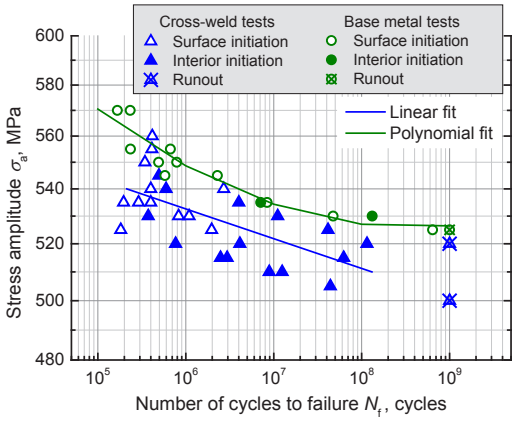

Fig. 2 *S–N* curves of the welded joint and pure base metal

3.2 Crack initiation behavior

Fig. 3 shows the morphologies of fatigue crack initiation of cross-weld specimens. A fatigue crack initiated from surface inclusion is observed at BM with the N_f of 4×10^5 cycles, as shown in fig. 3a; under similar N_f, the fatigue crack nucleated from interior pore with its boundary clearly shown in fig. 3b is observed at WM. Fig. 3c presents an interior fatigue cracking from non-metallic inclusion at WM in the VHCF regime where fatigue lifetime is longer. It is believed that the interior micro-defects being the crack initiation site is responsible for the disappearance of traditional fatigue limit. An enlarged observation around the inclusion illustrates the occurrence of fine granular area (FGA), according to Sakai et al. [19], with the characteristic of rough but fine surface. Here, the width of FGA at the radical direction is measured to be about 35 μm. The formation mechanisms of this kind of FGA in lower strength steels have been discussed in our previous paper with the help of microscopic observation based on FIB technique [20]. It was concluded that the FGA was actually polycrystalline grains formed due to continuously developed plastic energy around micro-defects [20].

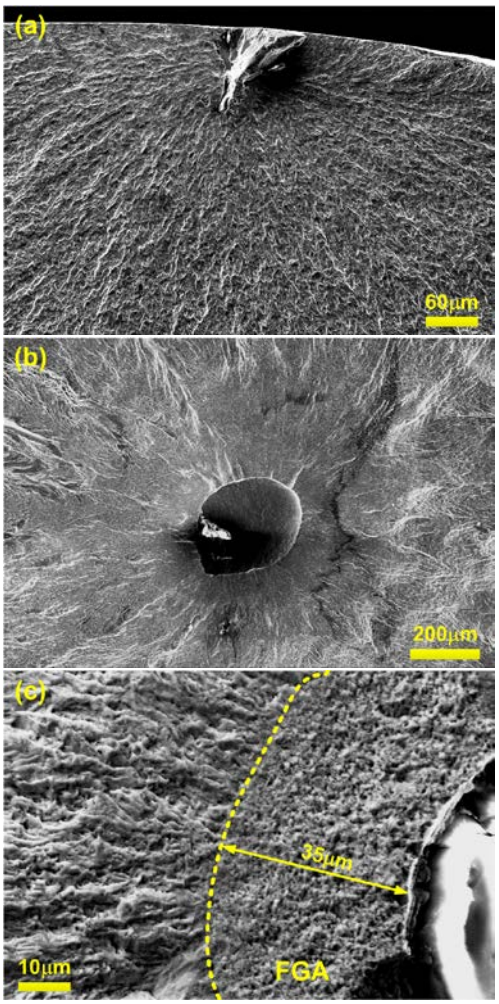

Fig. 3 Morphologies of fatigue crack initiation for cross-weld specimens: (a) crack initiation at the surface inclusion at BM (σ_a=540 MPa, N_f=4×10^5 cycles), (b) crack initiation at the interior pore at WM (σ_a=540 MPa, N_f=6×10^5 cycles) and (c) crack initiation at the non-metallic inclusion at WM (σ_a=525 MPa, N_f=4.15×10^7 cycles)

Fig. 4 shows the crack initiation behaviour of pure BM samples. As mentioned before, surface related fatigue cracking can even occur at extremely longer fatigue lifetimes, such as the one shown in fig. 4a, where a crack is formed from surface micro-defect with a N_f of

6.4×10^8 cycles. This may due to there are no larger interior defects. Fig. 4b presents crack initiation from a sub-surface inclusion which is different from the commonly observed fish-eye pattern. Another subsurface inclusion induced fatigue failure is shown in fig. 4c where the sample has the same stress level as the one in fig. 4a. This indicates that under such load amplitude, the fatigue crack can either initiate from specimen surface or subsurface micro-defect, which is the factor that dominates the variability of fatigue lifetime, and has the implication for the occurrence of fatigue limit for this kind of steel. A magnified view of the crack growth region on the fracture surface clearly indicates the striations, as illustrated in fig. 4d.

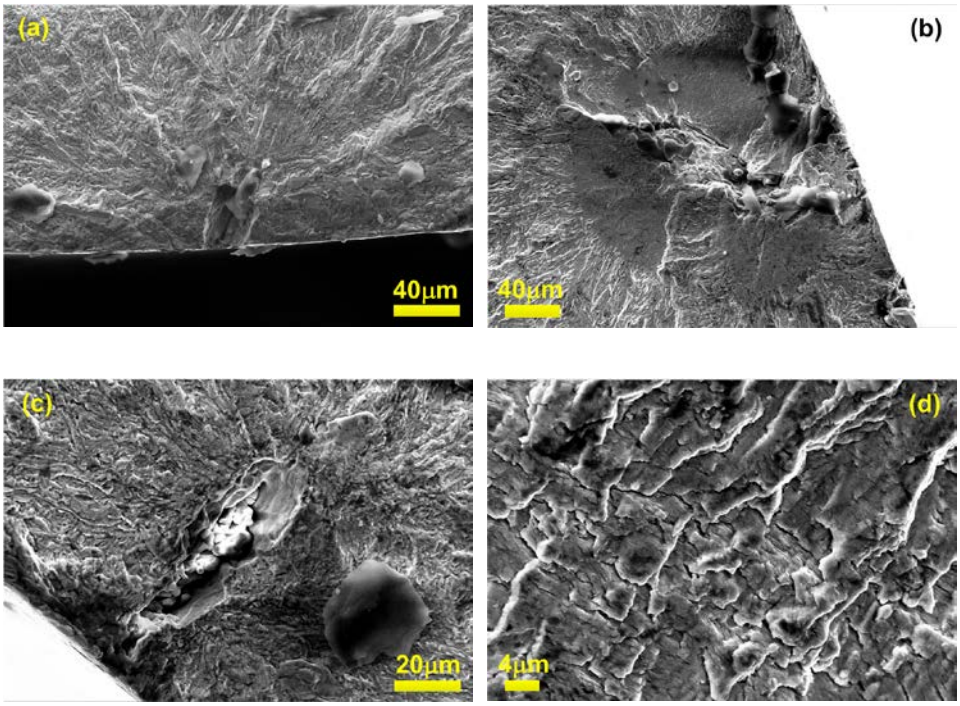

Fig. 4 Morphologies of fatigue crack initiation of pure BM samples: (a) surface inclusion (σ_a=525 MPa, N_f=6.4×10^8 cycles), (b) subsurface inclusion (σ_a=535 MPa, N_f=7.12×10^6 cycles), (c) subsurface inclusion (σ_a=525 MPa, N_f=4.15×10^7 cycles) and (d) striations formed at higher crack growth rate

3.3 Residual stress distribution along the welds

The X-ray diffraction method was applied to characterize the residual stress distribution along the welds. A XRD X350A residual stress analyser was used with a Cr Kα radiation tube with 2θ in the range of 163-149°. The residual stress was measured at selected points along the parallel section of the welds at the exposed surface. Moreover, a particular amount of surface layer was removed with the help of electrolytic polishing to measure residual stress at different depths, i.e., 10, 20 and 40 μm. Both axial and circumferential stresses were measured, and corresponding results are presented in fig. 5a. It is observed that the surface residual stress is mainly compressive in both the two directions. Axial stress varies from -190 MPa to -140 MPa, with higher values at the WM, whereas the circumferential stress is more compressive with the highest value (-252 MPa) also at the WM. Fig. 5b presents the residual stress distribution versus the depth of measurement at selected micro-zones along the welded joint. It is obvious that the compressive residual stress changes to positive at a distance of approximately 40 μm to the specimen surface, regardless of the points measured. This depth value has perfect consistence to the location of fatal inclusions shown in figs. 4b and 4c, which at least partly justifies the occurrence of sub-surface crack initiation behaviour. This also helps rationalize the transition of fatigue cracking from specimen surface to interior micro-defects [21]. Note the results reported here is a mixed case of residual stress originated from both welding and sample machining processes. The role of machining is to alter the initial residual stress state after welding, and after the stress relief heat treatment. The residual stress data presented here are original ones that do not consider the relaxation during cyclic loadings.

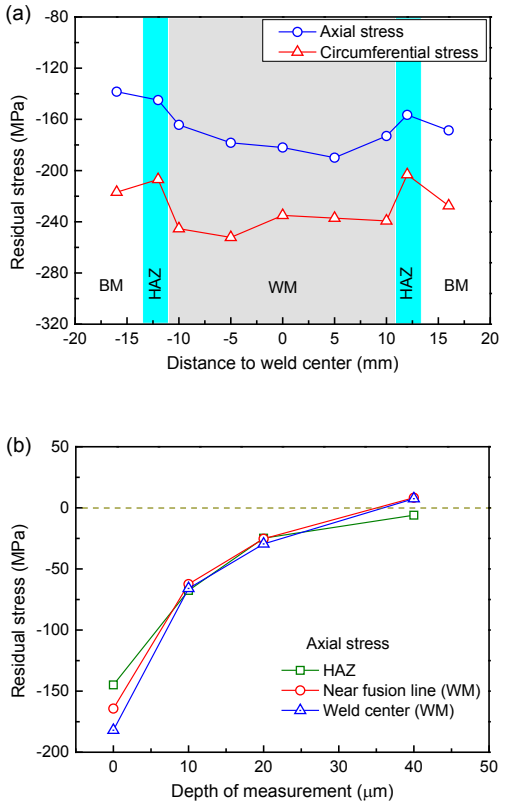

Fig. 5 Distribution of residual stress at specimen surface along the welded joint (a), and variation of axial residual stress with depth of measurement (b)

4 Discussion

4.1 Weld efficiency

As shown in fig. 2, the welded joint samples have lower fatigue strength than the pure BM ones. Fig. 6 depicts the FSRF, F, versus the fatigue lifetime. Here, F is calculated to be the ratio of fatigue strength value of welded joint samples to pure BM specimens. The value of F thus denotes the weld efficiency in terms of fatigue strength. It is apparent that the weld efficiency is not a constant value, but is varied with the fatigue lifetime. This is similar to the CSRF which is varied with temperature and time. Here, F is in the range of 0.95 to 0.976 for N_f in the range of 10^5 cycles to 10^9 cycles. It is observed that the F values in LCF and HCF regimes are different from those at ultra-long life regime. Most importantly, the F is found to be a function of fatigue lifetime. This has the implication of improving the current rules that are simply assuming constant FSRF. As shown in Fig. 6, with the increasing of N_f, F shows an increasing trend to the highest value of 0.976 at N_f of 9×10^6 cycles, after which the F is decreased. This has great significance in fatigue design of engineering structures and components in the VHCF regime where the conservativeness or allowance can be improved.

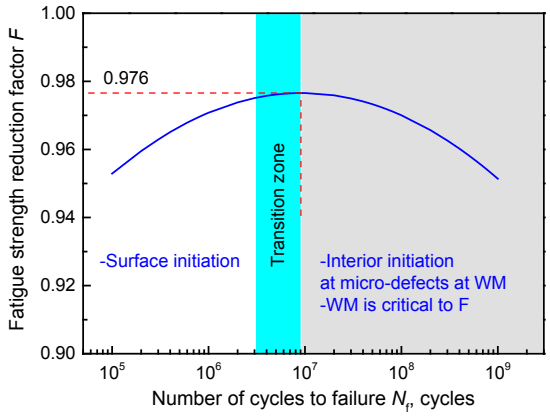

Fig. 6 Variation of fatigue strength reduction factor, F, with fatigue lifetime.

In this work, the underlying mechanisms for variation of weld efficiency with fatigue lifetime can be related with fatigue crack initiation modes of welded joint. It is interesting to find that the F is increased gradually in surface crack initiation dominated region, and continues increasing in the surface-to-interior transition region, and is finally decreased slowly for the dominant interior crack initiation at micro-defects at the WM. This means that the WM is the most critical to the FSRF in the VHCF regime, which implies that the design of components with ultra-long life requirement should consider the role of micro-defects in fatigue failure. *This is the first time to propose the role of micro-defect in fatigue design of a welded joint in the VHCF regime.* The questions of whether it is safe, whether it is conservative or non-conservative, when applying current fatigue design methods by extending the design life to VHCF regime, is yet unknown, unless with a full comparison.

4.2 Fatigue design of welds in current codes and standards

Current fatigue design codes for welded structures mainly include ASME Boiler and Pressure Vessel Code (i.e., Section III and Section VIII) [1], French code RCC-MR [2], BS 7608 [22], IIW recommendation [8], EN 1993-1-9: 2005 [23] and DNV-RP-C203 [24]. In this work, existing codes and standards on fatigue design of welded joint are compared based on the present test results.

4.2.1 ASME Boiler and Pressure Vessel Code

In the ASME Boiler and Pressure Vessel Code [1], fatigue design curves are based on *S-N* curves generated from smooth specimens of BM. In Section III, the fatigue design curves are obtained by applying a factor of 20 to fatigue cycles and 2 to stresses, based solely on engineering judgments. Moreover, weld efficiency is regarded as a stress intensification factor which accounts for the effects of local structural discontinuity (stress concentration) on the fatigue strength. While actually,

for welded joint, apart from the stress concentration due to geometry factor, fatigue strength reduction should also take account of weld imperfections, and weld residual stress. It is noted that, the practice of ASME Code is different from the case in other popular codes and standards where fatigue design of a particular welded joint is based on choosing one from a series of parallel *S-N* curves, in which process the FSRF is not fully represented. Dong et al. [25] tried to propose a master *S-N* curve for fatigue design of welded structures based on the discussion of fatigue strength reduction factor in ASME Code.

4.2.2 BS 7608

In the guide to fatigue design and assessment of steel products, BS 7608 [22], a general equation for *S-N* curve is listed as follows,

$$S_r^m N = C_0 \quad \text{(BS7608)} \tag{3}$$

where S_r is stress amplitude, N is the number of cycles, C_0 is a parameter defining the mean line S_r-N relationship, and m is the negative inverse slope of *S-N* curve. Here, the parameters for class C welds are selected and listed in Table 1. In case of fatigue design up to the ultra-long life regime, apart from the m and C_0 values, the standard provides a S_r of 102.27 MPa at N_f of 10^7 cycles, and keeps constant for longer fatigue lifetime. In the standard, the role of weld imperfections on the shape of *S-N* curves is not considered.

4.2.3 IIW recommendation

It is known that the fatigue resistance of a welded joint is limited by the fatigue resistance of the BM. As pointed out in IIW recommendation [8], when the fatigue assessment of classified structural details and welded joints is based on the nominal stress range, a fatigue class (FAT) of 112 is chosen here for transverse loaded butt welds. In case of very high cycle applications, m=3 for $1\times10^4 \le N \le 1\times10^7$ cycles and m=22 for $N>1\times10^7$ cycles is defined for the *S-N* curves [8]. By considering the residual stress effect, a fatigue enhancement factor $f(R)$ of 1.3 is applied here in case of R=-1 with medium residual stress, therefore, FAT is 145.6 MPa. The IIW recommendation also provides the guidelines for assessing the acceptance levels for porosity and inclusions in steel welds. The parameter for assessing inclusions is the maximum length. For a stress relieved welded joint, the maximum length of inclusion is 7.5 mm in case of the FAT is 100 MPa. In this work, the size of critical inclusions that are fatigue crack initiation sites is at the micro-meter level, as presented in Figs. 3 and 4. It is therefore inferred that the fatigue class should be higher than the highest value listed in the recommendation, that is, FAT >100 MPa.

In assessing the fatigue welds when considering the weld imperfections, for inner inclusions, the IIW recommendation offers a FAT of 71 for weld length less than 10 mm. This seems very conservative for fatigue assessment of welds as not all the inner micro-defects will be the failure site in the VHCF regime. The IIW recommendation does not provide the information of weld efficiency in case of fatigue assessment based on *S-N* curves of BM. It can be concluded that the current application of IIW recommendation to fatigue assessment of steel welds in the VHCF regime is either conservative or the role of micro-defects/weld efficiency is not adequately considered.

4.2.4 EN 1993-1-9:2005

The standard of EN 1993-1-9:2005 [23] also provides fatigue design curves up to the VHCF regime, where several parameters are defined. As listed in Table 1, the m is 3 for $N \le 5\times10^6$ cycles, and increased to 5 for $5\times10^6 \le N \le 1\times10^8$ cycles. For N higher than 1×10^8 cycles, the fatigue resistance is determined by the cut-off limit $\Delta\sigma_L$, which is 0.549 times of conventional fatigue limit at constant amplitude load, $\Delta\sigma_D$. According to the code, a detail category of 112, similar to the FAT 112 by IIW recommendation, is selected for transverse butt welds checked by NDT. Similarly, the EN code keeps the conservative style of fatigue assessment but keeps the role of micro-defect in the VHCF regime and weld efficiency unconsidered.

4.2.5 DNV-RP-C203

For the recommended practice of DNV-RP-C203 [24], the basic *S-N* curve is given as

$$\log N = \log \bar{a} - m \log \Delta\sigma \tag{4}$$

where $\log\bar{a}$ is intercept of $\log N$-axis by *S-N* curve, which takes the standard deviation of $\log N$ into account. As listed in Table 1, m is 3 for $N \le 10^7$ cycles while m is increased to 5 for $N \ge 10^7$ cycles. For transverse butt welds without backing strip, the weld detail category of C1 is selected here for *S-N* curves at air environment. The practice applies the traditional fatigue limit, and set the value at 65.5 MPa at N of 10^7 cycles. Note that choosing detail category of C1 is based on the understanding that overfill at weld toe is dressed flush without stress concentration, and failure is mainly related with weld defects. This means the *S-N* curve of the DNV code, though conservative for fatigue design of welds, considered the failure mode from micro-defects. No information of weld efficiency values are given in the recommended practice.

4.3 Fatigue design of welds for ultra-long life requirement

Fig. 7 shows a comparison of fatigue design curves of welds in current code and standards up to the VHCF regime. Note the fatigue data is specimen-based while in actual cases structural, environmental factors are involved. It is observed that all the design curves based on existing codes and standards are below the fatigue data of Cr-Ni-Mo-V steel welded joint. Severe conservativeness exists in BS7608, IIW recommendation, EN 1993-1-9: 2005 and DNV-RP-

C203, whose design curves are lying below the ASME and RCC-MR codes where fatigue design of welds is based on experimental data of BM. This means the design practice in ASME and RCC-MR codes are more reasonable than the simple procedure of selecting one among categorised *S-N* curves in other standards. This clearly indicates that design by current code and standards are very conservative, which will lead to costly over-design of welded structures and components. In other words, the current design practice is overloaded with safety factors by sacrificing engineering economics. This would partly explain the reasons why existing engineering components is still in use in a safe condition even the original design life has passed for several years.

The current code-based design needs improving due to over-conservatism. According to the tests results, design according to several stages of *S-N* curves with varied *m* values, i.e., the treatment in IIW recommendation, are not necessarily suitable for application into welded joints because the actual *S-N* curves may present a continuously decreasing shape. Whether it is a general rule or it is specimen-dependent has to be answered with in-depth further research. It seems there lacks a sound link between experimental results and modelling methods in codes. In this regard, how to incorporate the weld imperfections into modelling design curves is still an open issue. The criterion for defect assessment needs to be improved with an aim to differentiate the non-damaging defects from damaging ones under service loading conditions. The material defect based fatigue design for ultra-long life requirement, as proposed by Murakami [13, 16], is likely to reduce the conservativeness for fatigue design, if it could be extended into structure and component scales.

Table 1. Parameters in various codes and standards for fatigue design of steel welded joints

<table>
<tr><th>Codes and standards</th><th colspan="4">Parameters</th></tr>
<tr><td>ASME Section III</td><td colspan="4">Weld efficiency of 50% for fatigue design of welded joint</td></tr>
<tr><td>RCC-MR</td><td colspan="4">Weld efficiency of 80% for fatigue design of welded joint</td></tr>
<tr><td rowspan="2">BS7608, Class C</td><td>m</td><td>C_0</td><td>S_r, N_f=10^7 cycles</td><td>S_r, N_f=5×10^7 cycles</td></tr>
<tr><td>3.5</td><td>1.082×10^{14}</td><td>102.27</td><td>102.27</td></tr>
<tr><td rowspan="3">IIW, steel welded joint</td><td>m=3</td><td colspan="3">$10^4<N<1\times10^7$ cycles</td></tr>
<tr><td>m=22</td><td colspan="3">$N>1\times10^7$ cycles</td></tr>
<tr><td colspan="4">FAT 112 for transverse loaded butt weld, $f(R)$=1.3, and weld imperfections are considered</td></tr>
<tr><td rowspan="4">EN 1993-1-9: 2005, welded joint</td><td>m=3</td><td>$N\le5\times10^6$ cycles</td><td rowspan="3">$\Delta\sigma_D$ is constant amplitude fatigue limit at N=5×10^6 cycles, and $\Delta\sigma_L$ is cut-off limit at N=1×10^8 cycles.</td></tr>
<tr><td>m=5</td><td>$5\times10^6\le N\le1\times10^8$ cycles</td></tr>
<tr><td>$\Delta\sigma_L$=0.549$\Delta\sigma_D$</td><td>$N\ge1\times10^8$ cycles</td></tr>
<tr><td colspan="3">Detail category: 112 for transverse butt welds, and checked by NDT</td></tr>
<tr><td rowspan="3">DNV-RP-C203, welded joint</td><td>m=3</td><td>$N\le10^7$ cycles</td><td rowspan="2">Fatigue limit at N=10^7 cycles is 65.5 MPa;
$\log\overline{a_1}$=12.449, $\log\overline{a_2}$=16.081</td></tr>
<tr><td>m=5</td><td>$N\ge10^7$ cycles</td></tr>
<tr><td colspan="3">Detail category: C1 for transverse butt welds without backing strip, and the overfill is dressed flush without stress concentration, failure is mainly related with weld defects</td></tr>
</table>

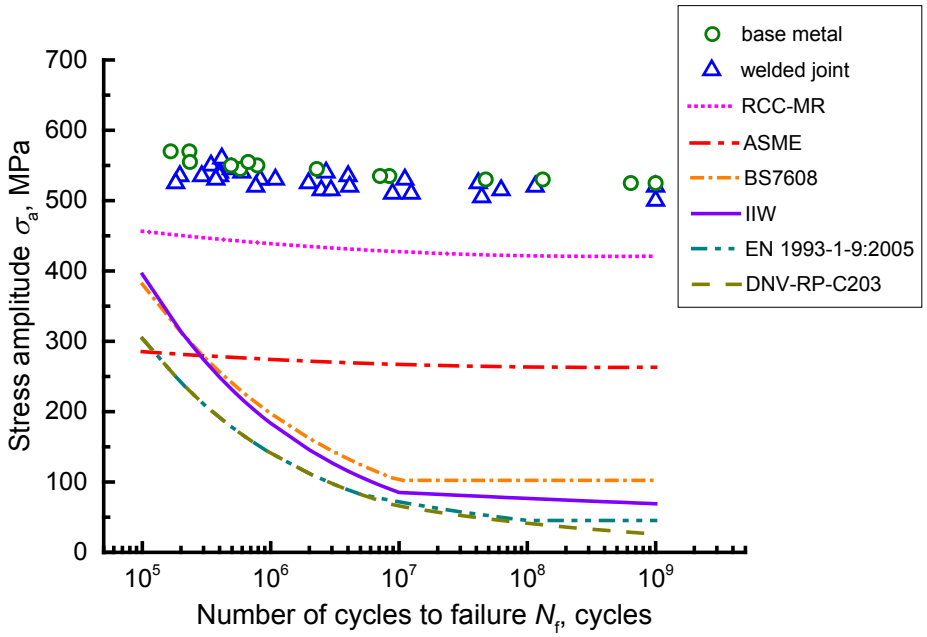

Fig. 7 A comparison of fatigue design curves in existing codes and standards up to the VHCF regime

5 Conclusions

In this paper, axially push-pull cyclic tests on a Cr-Ni-Mo-V steel welded joint were performed up to the VHCF regime under ultrasonic frequency at ambient temperature. Weld efficiency and fatigue design of the welded joint was discussed by comparing fatigue data with current codes and standards. The following conclusions can be reached.

(1) The weld efficiency in terms of fatigue strength reduction factor is found to be varied with fatigue lifetime for the first time. It increases from 0.95 in surface crack initiation dominated regime to the maximum value of 0.976 followed by gradually decreasing in interior micro-defects induced crack initiation in the VHCF regime.

(2) Current code-based fatigue design of welded joint is so conservative that would lead to costly over-design of engineering components, when comparing with experimental fatigue data. Any aims for improving the accuracy of current codes and standards should take account of weld imperfections for designing against fatigue of welds up to the ultra-long life regime.

Acknowledgements

The authors are grateful for the supports provided by the National Natural Science Foundation of China (51575182).

References

[1] ASME Boiler and Pressure Vessel Code, Section VIII, The American Society of Mechanical Engineers, 2004
[2] RCC MR Design Code, Section 1, French Society for Design and Construction Rules for Nuclear Island Components, 2002
[3] R. SandströM, S.T. Tu, J. Pres. Ves. Technol., 116, 76-80 (1994)
[4] S.-T. Tu, R. Sandström, Int. J. Pres. Ves. Piping, 57, 335-344 (1994)
[5] M.D. Mathew, S. Latha, K.B.S. Rao, Mater. Sci. Eng. A, 456, 28-34 (2007)
[6] M. Tabuchi, Y. Takahashi, Evaluation of Creep Strength Reduction Factors for Welded Joints of Modified 9Cr-1Mo Steel (P91), in: ASME 2006 Pressure Vessels and Piping/ICPVT-11 Conference, Vancouver, BC, Canada, 2006, pp. 529-534.
[7] Y. Takahashi, M. Tabuchi, J. Pres. Ves. Technol., 133, 021401-021401-021405 (2011)
[8] A. Hobbacher, *Recommendations for fatigue design of welded joints and components* (Springer, 2016)
[9] C.M. Sonsino, W. Fricke, F. De Bruyne, A. Hoppe, A. Ahmadi, G. Zhang, Int. J. Fatigue, 34, 2-16 (2012)
[10] D. Radaj, C.M. Sonsino, W. Fricke, Int. J. Fatigue, 31, 2-11 (2009)
[11] D. Radaj, C.M. Sonsino, W. Fricke, *Fatigue assessment of welded joints by local approaches* (Woodhead publishing, 2006)
[12] B. Pyttel, D. Schwerdt, C. Berger, Int. J. Fatigue, 33, 49-58 (2011)
[13] A. Roiko, Y. Murakami, Int. J. Fatigue, 41, 140-149 (2012)
[14] P.R. Fry, Eng. Fail. Anal., 46, 179-187 (2014)
[15] C.M. Sonsino, Int. J. Fatigue, 29, 2246-2258 (2007)
[16] Y. Murakami, Int. J. Fatigue, 41, 2-10 (2012)

[17] M.-L. Zhu, F.-Z. Xuan, Mater. Des., 65, 707-715 (2015)
[18] H.Q. Xue, E. Bayraktar, C. Bathias, J. Mater. Proces. Technol., 202, 216-223 (2008)
[19] T. Sakai, N. Oguma, A. Morikawa, Fatigue Fract. Eng. Mater. Struct., 38, 1305-1314 (2015)
[20] M.-L. Zhu, F.-Z. Xuan, Mech. Mater., 100, 198-208 (2016)
[21] M.-L. Zhu, F.-Z. Xuan, Y.-N. Du, S.-T. Tu, Int. J. Fatigue, 40, 74-83 (2012)
[22] BS 7608:2014+A1:2015, Guide to fatigue design and assessment of steel products, The British Standards Institution, 2015
[23] BS EN 1993-1-9:2005, Eurocode 3: Design of steel structures----Part 1-9: Fatigue, The British Standards Institution, 2005
[24] Recommended Practice DNV-RP-C203, Fatigue Design of Offshore Steel Structures, DET NORSKE VERITAS, 2008
[25] P. Dong, J.K. Hong, D. Osage, M. Prager, Welding in the World, 47, 31-43 (2003)